Fouling modeling in the ultrafiltration separation of oil emulsion from salty water

Elwira Tomczak[a], Wladyslaw Kaminski[a,*], Konrad Cwirko[b]

[a]*Faculty of Process and Environmental Engineering, Lodz University of Technology, Wolczanska 213, 90-924 Lodz, Poland, email: wladyslaw.kaminski@p.lodz.pl (W. Kaminski)*
[b]*Maritime University of Szczecin, Waly Chrobrego 1-2, 70-500 Szczecin, Poland*

ABSTRACT

Fouling may cause problems in the installations where ceramic membranes are used for the treatment of oily and saline waters. Therefore, research into oil separation and the fouling mechanism is expedient. The experimental research was carried out using oily and saline emulsions and a laboratory ultrafiltration apparatus equipped with a tubular ceramic membrane with a 300 kDa cut-off. The emulsions contained 500 or 1,500 ppm oil and 0.0%, 1.0%, or 3.5% NaCl, respectively. The transmembrane pressure applied was 0.05, 0.1, or 0.2 MPa while the linear flow velocity was set to 4, 5 or 6 m/s. The initial permeation flux J_0 was in a range from 12.0 to 14.8 [10^{-5} m^3/(m^2 s)]. The oil removal process proved successful. An average 97.13% rejection coefficient was achieved for the ultrafiltration trials. The study aimed to investigate and model the membrane fouling phenomenon in a modified approach. The main objective of the study was to identify the membrane fouling mechanism using the Hermia model. The classical approach approximates the experimental data with the linearized Hermia equation, determines the kinetic coefficients, and finds the most adequate out of four predetermined fouling mechanisms identified with previously assumed values of the n coefficient equal to 0, 1.0, 1.5, or 2.0. In the paper, it is postulated that n can be selected from the interval <0,2>. It means not only the main mechanisms mentioned above may take place but any transient states between these mechanisms exist or they may overlap each other. Additionally, remaining coefficients k_n, J_{ss} in Hermia's model was identified in the proposed numerical integration and optimization procedure.

Keywords: Ultrafiltration ceramic membrane; Hermia model; Fouling mechanism identification

1. Introduction

One of the most effective methods to remove oils in both emulsified and dispersed form is membrane filtration [1,2]. The advantages of using membrane processes are ease of process control, high cleaning efficiency, low investment costs [1,3]. The phenomenon of fouling is particularly important when removing oil emulsion from water. Oily and saline water is particularly difficult to handle. The place where, in large quantities, oily water is formed in a mixture with other salty water and other chemical substances are, for example, vessels, drilling rig. The oil concentration in such mixtures ranges from several hundred to several thousand ppm, while the salt concentration can be up to 300,000 ppm [4].

When ultrafiltration membranes are used, their filtration ability deteriorates with time which is reflected by the diminishing permeation flux. This deterioration is related mainly to the accumulation of dissolved and suspended solid particles/molecules on the outer surface of the membrane and within its pores or by the penetration of the solution/emulsion components into these pores. In

* Corresponding author.

general, the decline in hydraulic efficiency of the membrane is caused by the increasing flow resistance resulting from the phenomenon widely known as fouling. In membranes with smaller pores, the increase in resistance results primarily from the collection of components of the feed on the surface and in the pores of the membrane. Two main phenomena affect the mass transfer rate through the membrane known as concentration polarization and fouling [5].

Concentration polarization occurs when a boundary layer is formed in the vicinity of the membrane where there is a build-up in the concentration of non-permeating or slowly permeating components. As a result, the separation process becomes significantly slower usually, the separation ability of the membrane is also impaired [5].

The membrane fouling phenomenon has been known since the '50 s. It is still being researched with special attention to its causing and accelerating factors but also to the ways of counteracting and preventing membrane blocking. Fouling occurs mostly in porous membranes, that is, in micro-, ultra- and nanofiltration processes [6–10].

For the most part, membrane fouling depends on the size and the form of the substance present in the feed as well as the size of membrane pores. The other important factors are the interactions between the particles/molecules and between these particles/molecules and the membrane itself [2].

The limitations on mass transfer imposed by fouling are usually described with two different mathematical models [11].

The simplest approach is to use the relationship between the permeation flux and the transmembrane pressure which is the sum of the hydraulic resistance of a membrane and a resistance of fouling. This concept is known as the resistance in the series model. The resistances can be calculated based on experimental results [10,12].

The second approach to the identification of fouling mechanisms [8–10,13,14] rests on the concept introduced by Hermia [15]. In his paper, relying on the non-Newtonian fluid theory, Hermia gave mathematical relations for three types of particle accumulation and termed them the complete blocking filtration law, the standard blocking filtration law, and the intermediate blocking filtration law. To identify the fouling mechanism during dead-end micro-, ultra- or nanofiltration one can use the Hermia equation describing the decline in volumetric permeation flux with time:

$$\frac{d^2t}{dv^2} = k_n \left(\frac{dt}{dv} \right)^n \tag{1}$$

where t is the time of the ultrafiltration process (s), v is the volume of the permeate per membrane area (m³/m²), k_n is the phenomenological coefficient, n is the general coefficient (both depend on the fouling mechanism).

The above equation, valid for dead-end filtration performed under constant pressure, can be modified to suit cross-flow filtration in the following way [16,17]:

$$\frac{dJ}{dt} = -k_n \left(J - J_{ss} \right) J^{2-n} \tag{2}$$

This equation can be numerically or analytically integrated assuming the initial condition:

$$J(t_0) = J_0 \tag{3}$$

where J is the permeation flux [m³/(m²s)], J_{ss} is the asymptotic value of the permeation flux (steady-state flux) [m³/(m²s)].

In the paper, cross-flow filtration was considered since this is the case for laboratory and industrial applications.

Dead-end membrane filtration has been used for laboratory and medical filtration. The advantage of dead-end filtration is high product recovery and simple operation. The membrane, however, cannot be backwashed or cleaned because of internal pore blockage; instead, they are discarded. The fouling of a membrane is limited by shearing stress imposed by a stirrer located over the surface of the membrane.

Cross-flow membrane processes reverse osmosis, nanofiltration, ultrafiltration (UF), microfiltration the fluid to be filtered is fed parallel to the membrane. Fouling, in that case, is limited by the flow of the fluid and the membrane geometry.

In the Hermia model, depending on the pore-blocking mechanism, different values of n (Eqs. (1)–(3)) are accepted [17–19]:

- $n = 2$ for complete pore-blocking;
- $n = 1.5$ for standard (internal) pore-blocking;
- $n = 1$ for intermediate pore-blocking;
- $n = 0$ for cake filtration;

The approximate or exact solutions of the differential Eqs. (1) and (2) are given by many authors investigating the fouling phenomenon [8,20,21].

The analytical solutions of Eq. (2) with the initial condition (3) calculated for this study are gathered in Table 1. Eqs. (5) and (7) can be easily transformed into linear forms. Eq. (4), on the other hand, is entangled. In the subject literature for Eqs. (4) and (6) approximate forms are used.

To determine the leading pore-blocking mechanism, many authors linearize the equations either directly or approximately [17,22–25]. The solution that gives the best fit determines the fouling mechanism. Such an approach seems to be incorrect because the comparison between the respective fouling mechanisms is made in different coordinate systems whereas it should be made in a non-linear system, namely the <$t,J(t)$> coordinate system. Conducting a statistical assessment, for example, by calculating the determination coefficient (R^2) and the root mean square error (RSME), can then help find the most accurate solution.

The methods of identification offered by different authors distinguish only four types of the fouling mechanism. One may wonder whether any transient states between these mechanisms exist or whether they overlap each other. Assuming only four existing mechanisms and thus only four acceptable values of n in Eq. (2) seems a major simplification.

Fouling is much more complex and even for a single separated substance (with a defined molecular size), more than one particle deposition mechanism can come into play. Moreover, for multicomponent mixtures, fouling is certainly non-uniform and such a simple classification may fail [1,17]. In such cases, more sophisticated models

Table 1
Analytical solutions of Eq. (2) with the initial condition (3)

n	Integral of Eq. (2) with the condition (3)	Equation number
0	$$\frac{1}{J_{ss}^2}\ln\left(\frac{J(t)-J_{ss}}{J_0-J_{ss}}\left(\frac{J_0}{J(t)}\right)\right)+\frac{1}{J_{ss}}\left(\frac{1}{J(t)}-\frac{1}{J_0}\right)=-k_2 t$$	(4)
1.0	$$J(t)=\frac{J_{ss}}{1-\dfrac{J_0-J_{ss}}{J_0}\exp(-k_1 J_{ss}t)}$$	(5)
1.5	$$J(t)=J_{ss}\left(\frac{1+D}{1-D}\right)^2$$ $$D=\exp\left(-0.5\ J_{ss}^{0.5}k_{1.5}t+\ln\left(\frac{J_0^{0.5}-J_{ss}^{0.5}}{J_0^{0.5}+J_{ss}^{0.5}}\right)\right)$$	(6)
2.0	$$J(t)=J_{ss}+\left(J_0-J_{ss}\right)\exp(-k_2 t)$$	(7)

should be considered and examined with special attention to how well they reflect the accumulation of particles on the membrane when more than one mechanism is involved, simultaneously or successively.

2. Method proposed for identifying the fouling mechanism

It should be stated that, like in most physical mechanism classifications, there exist transient states. It means that there are pore blocking-mechanisms bordering on the four above-mentioned types. Consequently, the n coefficient in Eqs. (1) and (2) does not necessarily have to be equal to 0, 1.0, 1.5, or 2.0 but it may take values from the respective intervals: <0,1>, <1,1.5>, <1.5,2> and thus from the interval <0,2>.

Eq. (2) with the initial condition (3) can be integrated numerically with freely accepted accuracy for any value of n. For this reason, there is no need to set n to a predefined value such as 0, 1.0, 1.5, or 2.0.

To recognize the fouling mechanism, experiments should be carried out. Then, the experiments should allow the parameters k_n, J_{ss} and n to be calculated and therefore the final form of Eq. (2) to be unequivocally determined.

In this study, the experimental data were fitted by adjusting these coefficients with the help of a properly selected optimization method. As the optimization criterion, the minimum of the sum of squared deviations between experimental and calculated values with Eq. (8) was adopted. It was assumed that the n coefficient should have values from the interval <0,2> while k_n and J_{ss} should satisfy the inequalities $k_n > 0$ and $0 < J_{ss} < J_0$. Therefore, the experimental data were fitted to the results calculated with Eq. (2) employing constrained optimization:

$$\min_{X}\sum_{i=1}^{P}\left[J_{exp}(t_i)-J_{cal}(t_i)\right]^2 \tag{8}$$

where t_i is the time of the subsequent measurement; X is the set of allowed solutions; p is the number of experiments.

$$X=\begin{cases} n\in\langle 0,2\rangle \\ k>0 \\ 0<J_{ss}<J_0 \end{cases} \tag{9}$$

where $J_{cal}(t_i)$ can be determined by integrating Eq. (2) with the initial condition Eq. (3) for a defining moment in time t_i corresponding to the time of taking the subsequent permeate sample. Based on the calculated value of coefficient n, one can conclude about the fouling mechanism.

3. Experimental methodology

To verify the above-described approach, laboratory ultrafiltration of model oil–water-NaCl emulsions was performed using a ceramic tubular membrane. The goal was to achieve a possibly high permeation flux and high oil rejection.

The experimental emulsions having a volume of 10 dm^3 (the amount recommended by the producer of the UF apparatus) were prepared by mixing oil and water without NaCl and with NaCl in concentrations of 1 wt.% and 3.5 wt.%. In the homogenization process, HYDROL LHL 46 hydraulic oil was used. The emulsions were prepared using an ultrasonic Sonics VCX-500 apparatus (Sonics & Materials, Inc., Newtown, CT, USA) with the following operating parameters: frequency of 20 kHz, the peak-to-peak amplitude of the resonator oscillation of 124 μm, the resonator diameter of 13 mm, the temperature of 22°C, dispersion time of 5 s, oil injection directly into the resonator from a distance of about 5 mm, power density in the injection area of about 20 W/cm^2. In this way, emulsions containing 500 and 1,500 ppm oil and 0.0%, 1.0% and 3.5% NaCl, respectively, were prepared.

The emulsions were found to be stable, no phase separation was observed in the first 12 h. The emulsion droplet size measured with a laser analyzer (Beckman Coulter Co., Brea, CA, USA) varied from 0.3 to 1.5 μm (a log-normal distribution with $\mu = 0.587$ and $\sigma = 1.15$). In each case, the ultrafiltration test was done immediately after preparing the emulsion to avoid losing its homogeneity. The tests were performed in the following conditions: a linear flow velocity (LFV) of 4, 5, and 6 m/s, a transmembrane pressure (TMP) of 0.05, 0.1, and 0.2 MPa and a constant temperature of 20°C. The schematic diagram of the experimental ultrafiltration unit is presented in Fig. 1. The feed from the tank (1) is pumped (2) through a flow meter (4) to the membrane module (3). Retentate after the flow through the heat exchanger system and flow meter (6) is recycled to the feed tank. The use of heat exchangers takes place as needed – cooling, heating. The permeate after flowing through the flow meter is collected separately or recycled as well. Additionally, the installation is equipped with pressure and temperature gauges marked on the diagram.

The UF apparatus was equipped with a 23-channel ceramic membrane. The specification of the membrane is given in Table 2.

The unit was operated with a retentate and permeate recycle for 60 mins to stabilize the permeate flow rate. The samples were taken in 1 min and, at a later stage, in 10–15 min intervals. Each experiment was done twice.

The experiments were carried out according to a two-level factorial design [26]. The accepted values of the process parameters are gathered in Table 3. Discussion concerning the statistical evaluation of the effect of pressure, salinity, oil concertation, and velocity on permeation flux and rejection coefficient was not the subject of the paper. A detailed analysis of this issue was presented in the work [26].

The concentration of oil in the feed, the permeate, and the retentate samples were assessed by measuring their turbidity (Turbidimeter TN-100, Eutech Instruments, Singapore, Malaysia). The results were then recalculated to equivalent oil concentrations using the previously prepared calibration curve.

The concentration of salt in the samples was determined by measuring their specific conductivity with a laboratory multifunction meter CX-505. After each series of experiments, the membrane module and the UF apparatus were chemically cleaned according to the procedure recommended by the producer (120 min altogether) until the hydraulic permeability characteristic of a new membrane was retrieved.

The above-described experimental procedure helped determine the permeation flux as a function of time.

Table 2
Specification of the ceramic membrane

Property	Value
Cut-off (kDa)	300
Material	TiO_2/ZrO_2
Number of channels	23
Hydraulic diameter of the channel (m)	3.5×10^{-3}
Outer diameter (mm)	25
Length (mm)	1,178
Filtration area (m^2)	0.35
Burst pressure (MPa)	>9.0
Working pressure (MPa)	Max. 1.0
Chemical resistance	pH 0–14
Permeability to water ($dm^3/h/m^2/bar$)	450–500
Process temperature	<350°C
Steam sterilization	121°C for 30 min
Sterilization in an oxidizing environment	Yes
Resistance to solvents	Yes

Table 3
Design of experiments for the ultrafiltration of oil–water-NaCl emulsions

Experiment number	C_{oil} (ppm)	LFV (m/s)	TMP (MPa)	C_{NaCl} (%)
1	500	4	0.1	1
2	500	5	0.1	1
3	500	4	0.2	1
4	500	5	0.2	1
5	500	4	0.1	3.5
6	500	5	0.1	3.5
7	500	4	0.2	3.5
8	500	5	0.2	3.5
9	1,500	4	0.1	1
10	1,500	5	0.1	1
11	1,500	4	0.2	1
12	1,500	5	0.2	1
13	1,500	4	0.1	3.5
14	1,500	5	0.1	3.5
15	1,500	4	0.2	3.5
16	1,500	5	0.2	3.5
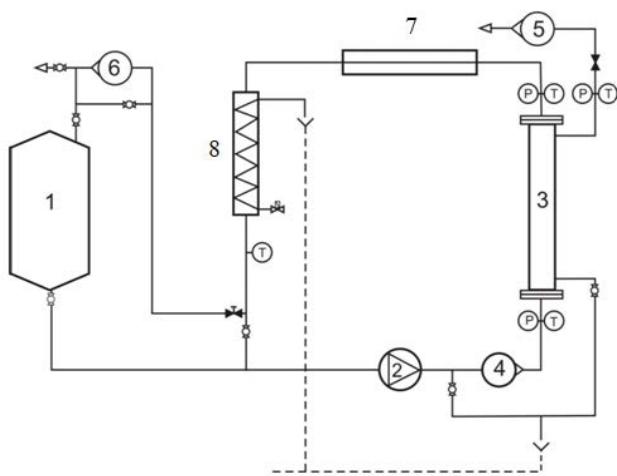
Fig. 1. Laboratory UF unit with a tubular ceramic membrane: (1) feed tank; (2) pump; (3) tubular ceramic membrane; (4–6) flow meters; (7) heat exchanger (heating function); (8) heat exchanger (cooling function).

The volume flux of permeate was calculated with Eq. (10):

$$J_V = \frac{1}{A}\frac{dV}{dt} \tag{10}$$

where J_V is the volume flux [m³/(m² s)], V is the permeate volume (m³), A is the membrane area (m²), t is the time (s).

The rejection coefficient was calculated using Eq. (11):

$$r = \left(1 - \frac{C_P}{C_F}\right) \times 100\% \tag{11}$$

where C_F is the oil concentration in the feed (ppm), C_P is the oil concentration in the permeate (ppm).

4. Optimization calculations for the identification of the fouling mechanism

The optimization calculations were carried out according to the methodology described in Section 2 of this paper, using the MATLAB *fmincon* procedure that searches for the objective function minimum using the constrained gradient method.

Eq. (2) was solved numerically. For this purpose, the fifth-order Runge–Kutta integration method was applied. The integration was done using the 'ode45' procedure.

In Tables 4 and 5 calculated coefficient k_n, J_{ss}, and $n = n_{cal}$ from optimization procedure were presented.

The last columns in Tables 4 and 5, denoted by n_{final} represents rounded values attributed to a certain fouling mechanism. In most cases, the membrane is blocked in two stages. Initially, the separated particles/molecules gradually accumulate on the membrane surface and in its pores (simultaneously or successively) following the first three fouling mechanisms. The initial blockage of the pores often causes irreversible fouling of the membrane and reduces its filtration ability. Continuing the process without restoring the membrane surface to the initial state (either mechanically, chemically, or by the inflowing feed stream) leads to multi-layered accumulation of particles and the creation of the filtration cake [22,27].

In half of the experiments done with the 500 ppm oil concentration, the complete pore blocking was identified (n_{final} = 2), in three experiments the forming of the filtration cake was recognized (n_{final} = 0) and in one experiment the n_{final} value was found to be 0.2. Therefore, one can surmise that a mixed mechanism came into play, preceded by, for example, complete blocking and being in part included in the creation of the filtration cake.

The experiments where the n coefficient took a value of zero or close to zero were performed under a TMP of 0.2 MPa and were not influenced by the concentration of salt.

When the concentration of oil in the emulsion was higher (1,500 ppm) the complete pore blocking mechanism was identified (n_{final} = 2) along with the mechanism approaching complete blocking (n_{final} = 1.88) (experiment No. 14). In these tests, the oil concentration was a major contribution.

Table 4
Optimum coefficients in Eq. (2) calculated for 500 ppm oil

Experiment number	k [unit depends on n]	J_{ss} [10⁻⁵ m³/(m² s)]	n_{cal}	n_{final}
1	8.15×10^{-2}	7.52	1.999	2.0
2	7.84×10^{-2}	7.07	1.999	2.0
3	3.58×10^{-4}	14.01	7.08×10^{-4}	0
4	5.06×10^{-4}	13.53	5.68×10^{-3}	0
5	8.04×10^{-2}	6.69	1.999	2.0
6	5.24×10^{-2}	6.44	1.999	2.0
7	8.81×10^{-4}	12.78	0.189	0.2
8	6.05×10^{-4}	12.40	5.28×10^{-4}	0

Table 5
Optimum coefficients in Eq. (2) calculated for 1,500 ppm oil

Experiment number	k [unit depends on n]	J_{ss} [10⁻⁵ m³/(m² s)]	n_{cal}	n_{final}
9	1.52×10^{-2}	6.04	1.998	2.0
10	1.88×10^{-2}	6.60	1.985	2.0
11	1.52×10^{-2}	12.70	1.990	2.0
12	1.61×10^{-2}	11.2	1.999	2.0
13	2.17×10^{-2}	6.00	1.999	2.0
14	1.34×10^{-2}	6.00	1.877	1.88
15	1.83×10^{-2}	12.00	1.985	2.0
16	1.46×10^{-2}	11.20	1.999	2.0

It is possible that the blocking of the pores was intensified by lowering the flow rate.

The experiments where the n coefficient took a value of zero or close to zero were performed under a TMP of 0.2 MPa and were not influenced by the concentration of salt.

The optimization results were evaluated statistically. The determination coefficient R^2, Eq. (12) and the RSME δ, Eq. (13) were adopted as measures of the approximation accuracy.

$$R^2 = 1 - \frac{\sum_{i=1}^{P}\left(J_{i\exp} - J_{i\cal}\right)^2}{\sum_{i=1}^{P}\left(J_{i\exp} - J_{m}\right)^2} \tag{12}$$

$$\delta = \sqrt{\frac{\sum_{i=1}^{P}\left(J_{i\exp} - J_{i\cal}\right)^2}{P}} \tag{13}$$

The results of the statistical evaluation are gathered in Tables 6 and 7.

Tables 6 and 7 confirm that the implemented calculation procedure produced acceptable results. The coefficient of determination took values from between 0.922 and 0.995. For 500 ppm oil, the best approximation was obtained for experiment No. 5 where $R^2 = 0.995$ and $\delta = 0.0176$ [10^{-5} m^3/(m^2 s)]. The best results for 1,500 ppm oil were $R^2 = 0.972$ and $\delta = 0.0844$ [10^{-5} m^3/(m^2 s)], respectively (experiment No. 11).

The exemplary results of the measurements and the optimization are presented in Figs. 2–7. In these figures, the data points are denoted by symbols while the approximating function is plotted with a solid line. The fitting curves were calculated using coefficients collected in Tables 4 and 5.

The figures demonstrate that the separation of oil from water and NaCl, executed with a ceramic membrane (300 kDa), brought satisfying results in terms of the filtration flux. After a very sharp decline from about 4%–18% in the first 20 min, the flux stabilized during the next 40 min.
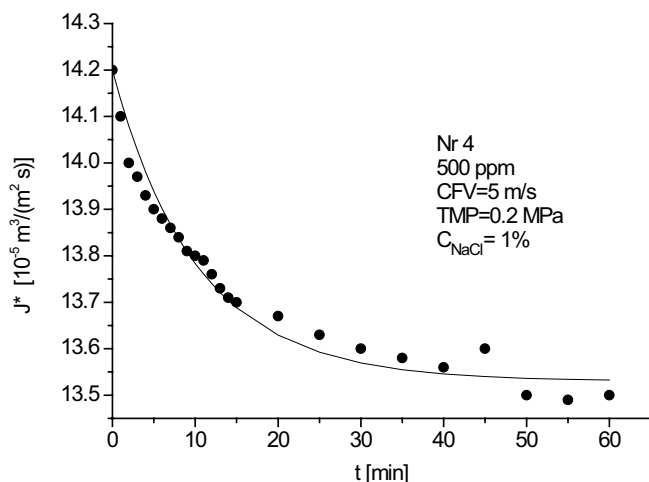
This behavior points to good efficiency and the possibility of building a more complex oil removal apparatus equipped with a ceramic membrane. A very high rejection coefficient for all the experiments (from 91.4% to 99.2% and 97.13% on average) confirms a good choice of membrane.

The highest value of the rejection coefficient $R = 99.2\%$ was achieved in experiment No. 22 (500 ppm oil) while for 1,500 ppm oil the highest value of R, equal to 98.8, was achieved in experiment No. 13. The high oil rejection was accompanied by good process efficiency. The highest initial permeation flux was obtained under a TMP of 0.2 MPa, regardless of the concentrations of oil and salt. The J_0 flux values were from 12.0 to 14.8 [10^{-5} m^3/(m^2 s)].

Experiment No. 4 is significant from the perspective of both efficiency and selectivity. In this experiment, performed with the following parameters LFV = 5 m/s, TMP = 0.2 MPa, C_{NaCl} = 1% and C_{oil} = 500 ppm, a rejection of 98.8% was achieved along with the highest initial flux J_0 of 14.8
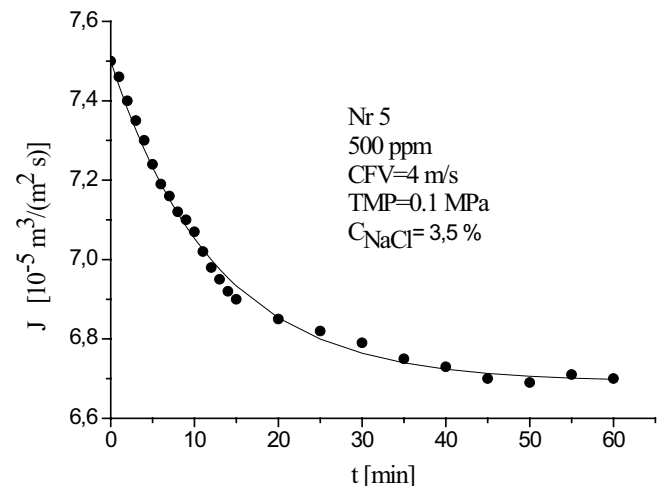
Fig. 3. The experimental points and the fitting curve for experiment No. 5.

Fig. 2. The experimental points and the fitting curve for experiment No. 4.
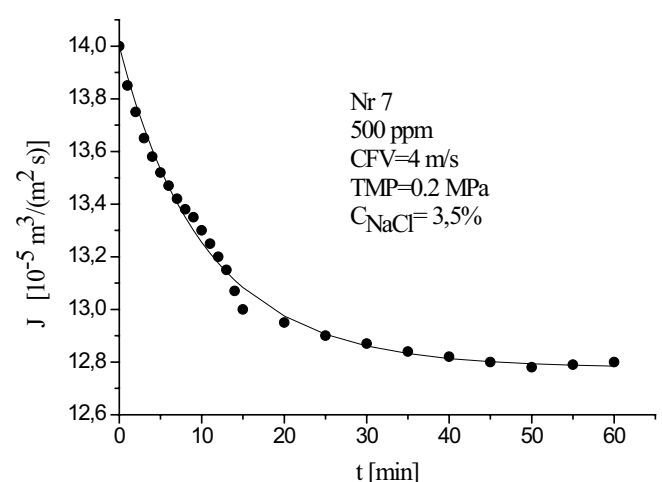
Fig. 4. The experimental points and the fitting curve for experiment No. 7.
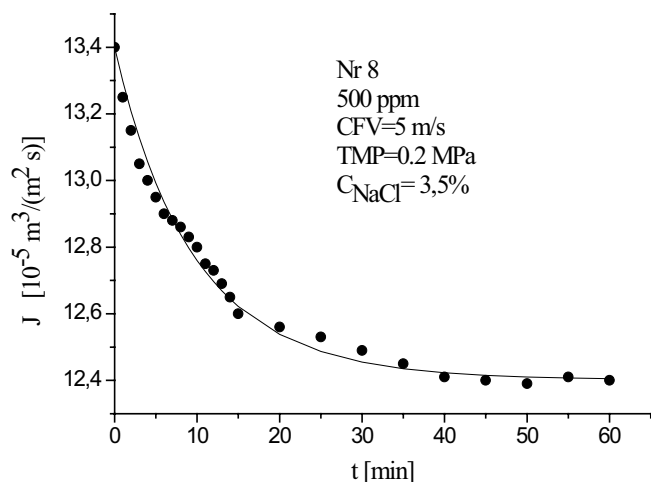
Fig. 5. The experimental points and the fitting curve for experiment No. 8.
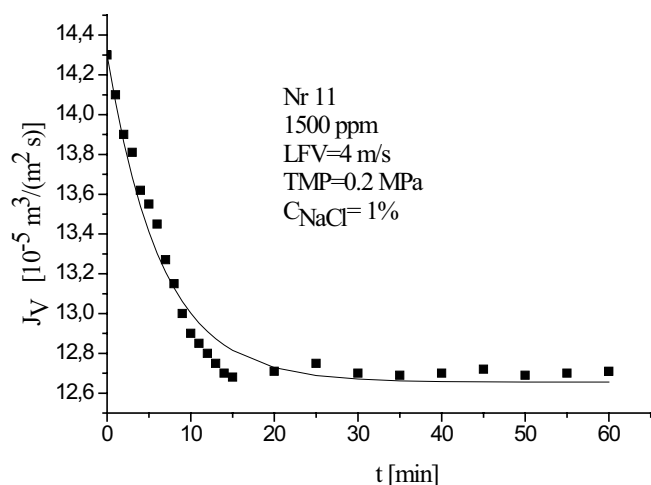
Fig. 6. The experimental points and the fitting curve for experiment No. 11.
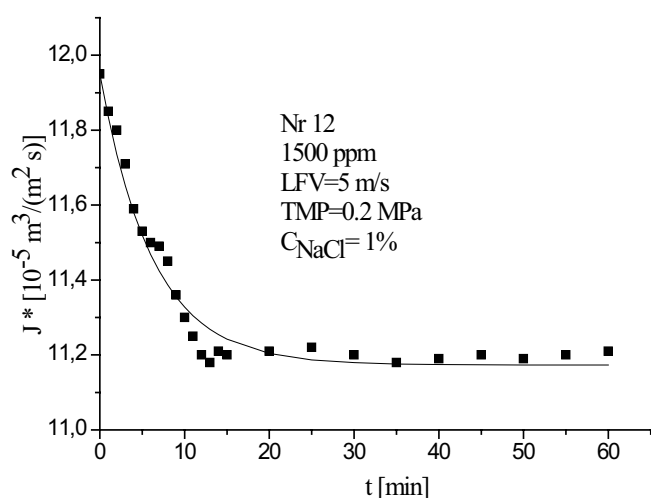
Fig. 7. The experimental points and the fitting curve for experiment No. 12.

Table 6
Statistical assessment of the optimization for 500 ppm oil

Experiment number	R^2	δ [10^{-5} m³/(m² s)]
1	0.975	0.020
2	0.955	0.030
3	0.958	0.046
4	0.965	0.035
5	0.995	0.018
6	0.983	0.035
7	0.993	0.030
8	0.986	0.034

Table 7
Statistical assessment of the optimization for 1,500 ppm oil

Experiment number	R^2	δ [10^{-5} m³/(m² s)]
9	0.953	0.081
10	0.931	0.044
11	0.972	0.084
12	0.962	0.046
13	0.932	0.077
14	0.933	0.042
15	0.962	0.100
16	0.922	0.092

[10^{-5} m³/(m² s)] and the steady-state flux J_{ss} (measured after the stabilization period) equal to 13.53 [10^{-5} m³/(m² s)].

5. Conclusions

- This paper proposes a method for identifying the membrane fouling mechanism by solving the Hermia equation numerically and using the optimization procedure. This new approach consists not in accepting the a priori values of the exponential factor n but rather in calculating this value with the assumption that it comes from the interval <0,2>.
- Fitting the experimental data using the proposed mathematical model gives a good approximation for all stages of the process and, based on the calculated value of the exponential factor n, and k_n, J_{ss} coefficients allows the governing fouling mechanism to be identified, even if other, simultaneous or successive, mechanisms occur.
- In that particular case of oil emulsion separation from saline water, two leading cases $n = 0$ (cake filtration) or $n = 2$ (complete pore-blocking) were obtained as a result of the proposed procedure. Also, two particular results $n = 0.2$ and 1.88 were found.
- The ultrafiltration experiments performed in this study, using a ceramic membrane, can be considered efficient. The recorded initial permeation flux J_0 was in a range from 12.0 to 14.8 [10^{-5} m³/(m² s)]. A very high rejection coefficient was also achieved in all the experiments, giving an average of 97.13%.

Symbols

A — Membrane area, m^2
C_{oil} — Oil concentration, ppm
C_P — Oil concentration in permeate, ppm
C_F — Oil concentration in feed, ppm
C_{NaCl} — Salt concentration, %
D — Variable defined by Eq. (6), –
k_n — Phenomenological coefficient, dependent on n
J — Permeation flux, m^3/(m^{2}s)
LFV — Linear flow velocity, m/s
n — General coefficient (dependent on the fouling mechanism), –
p — Number of experiments, –
R^2 — Determination coefficient, –
t — Time of the ultrafiltration process, s
TMP — Transmembrane pressure, MPa
v — Volume of the permeate per membrane area, m^3/m^2
V — Permeate volume, m^3
X — Set of allowed solutions
δ — Root mean square error, m^3/(m^{2}s)
μ — Mean value
σ — Standard deviation
ξ — Variable defined by Eq. (A6)

Subscripts

0 — Initial
cal — Calculated
exp — Experimental
final — Final
i — Subsequent moment
m — Mean
ss — Asymptotic

References

[1] Y.-M. Lin, G.C. Rutledge, Separation of oil-in-water emulsions stabilized by different types of surfactants using electrospun fiber membranes, J. Membr. Sci., 563 (2018) 247–258.

[2] S.L. Huang, R.H.A. Ras, X.L. Tian, Antifouling membranes for oily wastewater treatment: Interplay between wetting and membrane fouling, Curr. Opin. Colloid Interface Sci., 36 (2018) 90–109.

[3] G. Mustafa, K. Wyns, A. Buekenhoudt, V. Meynen, Antifouling grafting of ceramic membranes validated in a variety of challenging wastewaters, Water Res., 104 (2016) 242–253.

[4] A.R. Pendashteh, L.C. Abdullah, A. Fakhru'l-Razi, S.S. Madaeni, Z.Z. Abidin, D.R.A. Biak, Evaluation of membrane bioreactor for hypersaline oily wastewater treatment, Process Saf. Environ. Prot., 90 (2012) 45–55.

[5] C. Rey, N. Hengl, S. Baup, M. Karrouch, A. Dufresne, H. Djeridi, R. Dattani, F. Pignon, Velocity, stress and concentration fields revealed by micro-PIV and SAXS within concentration polarization layers during cross-flow ultrafiltration of colloidal Laponite clay suspensions, J. Membr. Sci., 578 (2019) 69–84.

[6] E.J. de la Casa, A. Guadix, R. Ibáñez, E.M. Guadix, Influence of pH and salt concentration on the cross-flow microfiltration of BSA through a ceramic membrane, Biochem. Eng. J., 33 (2007) 110–115.

[7] H.A. Mousa, S.A. Al-Hitmi, Treatability of wastewater and membrane fouling, Desalination, 217 (2007) 65–73.

[8] B.G. Choobar, M.A.A. Shahmirzadi, A. Kargari, M. Mano-uchehri, Fouling mechanism identification and analysis in microfiltration of laundry wastewater, J. Environ. Chem. Eng., 7 (2019) 103030, https://doi.org/10.1016/j.jece.2019.103030.

[9] A.Y. Kirschner, Y.-H. Cheng, D.R. Paul, R.W. Field, B.D. Freeman, Fouling mechanisms in constant flux crossflow ultrafiltration, J. Membr. Sci., 574 (2019) 65–75.

[10] G.D. Arend, K. Rezzadori, L.S. Soares, J.C.C. Petrus, Performance of nanofiltration process during concentration of strawberry juice, J. Food Sci. Technol., 56 (2019) 2312–2319.

[11] S. Judd, B. Jefferson, Membranes for Industrial Wastewater Recovery and Reuse, Elsevier, Oxford, 2003.

[12] K. Ćwirko, E. Tomczak, D. Szaniawska, Membrane fouling in the ultrafiltration of water–protein–sodium chloride model systems, Chem. Process. Eng., 39 (2018) 185–196.

[13] W.X. Zhang, L.H. Ding, Investigation of membrane fouling mechanisms using blocking models in the case of shear-enhanced ultrafiltration, Sep. Purif. Technol., 141 (2015) 160–169.

[14] B.M. Harouna, O. Benkortbi, S. Hanini, A. Amrane, Modeling of transitional pore blockage to cake filtration and modified fouling index – dynamical surface phenomena in membrane filtration, Chem. Eng. Sci., 193 (2019) 298–311.

[15] J. Hermia, Constant pressure blocking filtration laws–application to power-law non-Newtonian fluids. Tran. Inst. Chem. Eng., 60 (1982) 183–187.

[16] R. Field, Fundamentals of Fouling: Membrane Technology, K.-V. Peinemann, S.P. Nunes, Eds., Membranes for Water Treatment, Wiley-VCH, Weinheim, New York, Brisbane, Singapore, Toronto, 2010

[17] E. Iritani, N. Katagiri, Developments of blocking filtration model in membrane filtration, KONA Powder Part. J., 33 (2016) 179–202.

[18] V.B. Brião, C.R.G. Tavares, Pore blocking mechanism for the recovery of milk solids from dairy wastewater by ultra-filtration, Braz. J. Chem. Eng., 29 (2012) 393–407.

[19] M. Abbasi, A. Taheri, Modeling of coagulation-microfiltration hybrid process for treatment of oily wastewater using ceramic membranes, J. Water Chem. Technol., 236 (2014) 80–89.

[20] S.M. Heidari, M. Amirinejad, H. Jahangirian, Investigation of fouling mechanisms using surface morphology and physicochemical membrane features, Chem. Eng. Technol., 42 (2019) 1310–1320.

[21] S.P. Sundaran, C.R. Reshmi, P. Sagitha, O. Manaf, A. Sujith, Multifunctional graphene oxide loaded nanofibrous membrane for removal of dyes and coliform from water, J. Environ. Manage., 240 (2019) 494–503.

[22] M.I.N.H. Amin, A.W. Mohammad, M. Markom, L.C. Peng, N. Hilal, Analysis of deposition mechanism during ultrafiltration of glycerin-rich solutions, Desalination, 261 (2010) 313–320.

[23] S. Saha, C. Das, Analysis of fouling characteristics and flux decline during humic acids batch ultrafiltration, J. Chem. Eng. Process Technol., 6 (2015) 1–7.

[24] N. Aryanti, D.H. Wardhani, S. Supandi, Flux profiles and mathematical modeling of fouling mechanism for ultrafiltration of konjac glucomannan, Chem. Chem. Eng. Biochem. Food Ind., 17 (2016) 125–137.

[25] X. Zou, J. Li, On the fouling mechanism of polysulfone ultrafiltration membrane in the treatment of coal gasification wastewater, Front. Chem. Sci. Eng., 10 (2016) 490–498.

[26] E. Tomczak, W. Kaminski, K. Cwirko, Two-level factorial experiments in the ultrafiltration of oil–water emulsions, Desal. Water Treat., 128 (2018) 119–124.

[27] B. Sarkar, A combined complete pore blocking and cake filtration model during ultrafiltration of polysaccharide in a batch cell, J. Food Eng., 116 (2013) 333–343.